Journal of Applied Polymer Science

Thermal, Optical, and Electrical Characterization of Thin Film Coated RTV 655 Bilayer System

Firouzeh Sabri,[1] Derek S. King,[2] Abhi Lokesh,[3] Chris J. Hatch,[4] Randolph A. Duran[5]

[1]Department of Physics, University of Memphis, Memphis, Tennessee 38152
[2]Missouri University of Science and Technology, Rolla, Missouri 65409
[3]Department of Chemistry, University of Florida, Gainesville, Florida 32611
[4]Department of Physics, University of Memphis, Memphis, Tennessee 38152
[5]Department of Chemistry, Louisiana State University, Baton Rouge, Louisiana 70803
Correspondence to: F. Sabri (E-mail: fsabri@memphis.edu)

ABSTRACT: Adhesion of thin films to hydrophobic elastomeric substrates is of particular interest in the area of flexible electronics and nano-sensor technology. Here, nanometer-thick Au films were deposited directly onto hydrophobic RTV 655 substrates by means of sputtering, thermal evaporation, and electroless techniques without an adhesion-promoting layer. The bilayer system was exposed to repeat thermal cycling and changes to the surface morphology of the thin film were monitored electrically and optically. Buckle formation in the as-deposited film was attributed to stress in the film and substrate stiffness rather than thermal coefficient mismatch between films. The Au-RTV 655 interface was water tight and maintained a strong adhesion despite repeated thermal cycles. Sputtered and thermally evaporated carbon-coated RTV 655 substrates were also studied in parallel for comparison. Periodic arrays of buckles formed in pre-strained RTV 655 samples showed reproducibility in their optical properties demonstrating good adhesion between the two layers without an interfacial layer. © 2014 Wiley Periodicals, Inc. J. Appl. Polym. Sci. **2015**, *132*, 41396.

KEYWORDS: applications; elastomers; films; surfaces and interfaces

Received 2 April 2014; accepted 4 August 2014
DOI: 10.1002/app.41396

INTRODUCTION

Electronic components such as semiconductor and MEMS devices fabricated on rigid solid state substrates have limited applications due to the low strain at failure (<1%)[1] of these materials. Elastomeric materials on the other hand are versatile polymers used for a variety of applications such as encapsulation and insulation,[2,3] shock absorption,[4] artificial skin,[5] flexible opto-electronics,[6] and calibration targets for the Mars rovers.[7,8] A critical step in the design and fabrication of devices on compliant substrates is the metallization stage which can be a challenge due to the inherent hydrophobic nature and low surface energy of these materials. Good adhesion between thin (nm-thickness) metal layers and compliant polymeric substrates have been known to lead to significantly high strain tolerances without disconnect in the conductive layer and delamination between the two layers.[9–11] Adhesion of metal films—in particular noble metals—to such hydrophobic substrates has been addressed by using an adhesion-promoting layer such as Cr[12,13] or Al/Al_2O_3.[14] Complications associated with introducing adhesion layers include an extra processing step and expansion coefficient mismatch between the various layers leading to undesired film buckling.[15–17] Most common deposition techniques include thermal evaporation, sputtering, and electroless deposition[18–20] each with inherent advantages and limitations. Elastomeric substrates of the room temperature vulcanizing (RTV) family such as RTV 655, RTV 615, and Sylgard 184 are attractive materials for applications mentioned earlier. Their tunable electrical, mechanical, and optical properties as well as chemical stability allows for unique substrate designs with specific properties relevant to the application in mind. The temperature range of operation and low temperature flexibility however is limited for most for these room temperature vulcanizing polymers with the exception of RTV 655 where an operating range of −115 to 204°C can be expected.[8] Additionally, the chemical makeup of RTV 655 allows for better stability under exposure to ionizing radiation such as ultraviolet radiation leading to broader applications for the RTV 655 formulation than others.

In this work, gold (Au) + RTV 655 bilayer systems were created by means of sputtering, thermal evaporation, and electroless deposition without the use of an adhesion-promoting layer. The optical, mechanical, and electrical behavior of the bilayer system was investigated and characterized under different conditions

with a specific emphasis on the formation of buckles in the deposited films. Carbon (C) − RTV 655 bilayer systems were also created and studied in parallel for comparison.

MATERIALS AND METHODS

Preparation of RTV 655 Substrates

Pigmented (opaque) RTV 655 samples of dimensions 6 × 40 × 20 mm^3 and 3 × 40 × 20 mm^3 ($H \times L \times W$) were prepared according to the method discussed in detail previously[8] and cured at 90°C in custom-designed aluminum molds, according to the manufacturer's recommendations. Once cured, the samples were removed from the molds and cleaned in acetone and isopropyl alcohol (IPA) beakers for 1 min each in an ultrasound bath, then fully dried with a nitrogen gun and stored under airtight conditions until the next step. Corning cover slips were cleaned in a similar manner and dried under the same conditions. The surfaces of all the cured samples were checked by an optical microscope and subsequently by a Veeco atomic force microscope (AFM) in tapping mode to ensure that the surfaces were flat and that no pre-existing patterns or periodic surface defects were present.

Thin Film Deposition

Sputter Deposition. *Relaxed substrates*: cleaned RTV 655 samples (cut into 20-mm wide polymer strips) and Corning cover slips (control) prepared in the section "Preparation of RTV 655 Substrates" were transferred to an ion bench-top sputter coater with 99.999% gold (Au) target (EMS Sciences). Polymer samples were carefully placed on glass slides in order to prevent handling and the application of any stress post the thin film deposition stage. The chamber was pumped down to a pressure of 1 × 10^{-1} mbar and 40 nm of Au was sputtered after which the chamber was vented using pure argon (Ar) gas. Polymer surfaces were either coated (1) uniformly with full coverage (FC) or, (2) through shadow masking where a series of 3-mm wide parallel channels (PC) were created. In this case, custom-made aluminum (Al) masks shown in Figure 1(a) were created in-house in order to form the parallel channels. After sputtering, the masks were carefully removed without damaging the sputter-coated film underneath.

Strained substrates: sputter deposition on strained samples was performed by first inserting the 20-mm wide polymer strips in a custom-built 1-D extender and securing the two ends of the polymer between the two grips at either end, without over tightening the threads. The polymer samples were then strained uniaxially by 15% (maximum strain possible with the extender) and subsequently transferred to the sputter coating chamber while under strain. As before, 40 nm of Au was sputter-deposited. Upon completion of the sputtering stage the mask was removed (Figure 1(b)) and the strain on the sample was released gradually while observing the sample under the objective of a reflective light microscope. Highly ordered buckles here on referred to as "accordion" style began to form instantly. Both FC and PC samples were created (Figure 1).

Ion Beam Deposition of Carbon. Relaxed (0% strain) RTV 655 substrates were loaded into a Gatan Model 681 Ion Beam Coater containing a 99.999% carbon target. Approximately

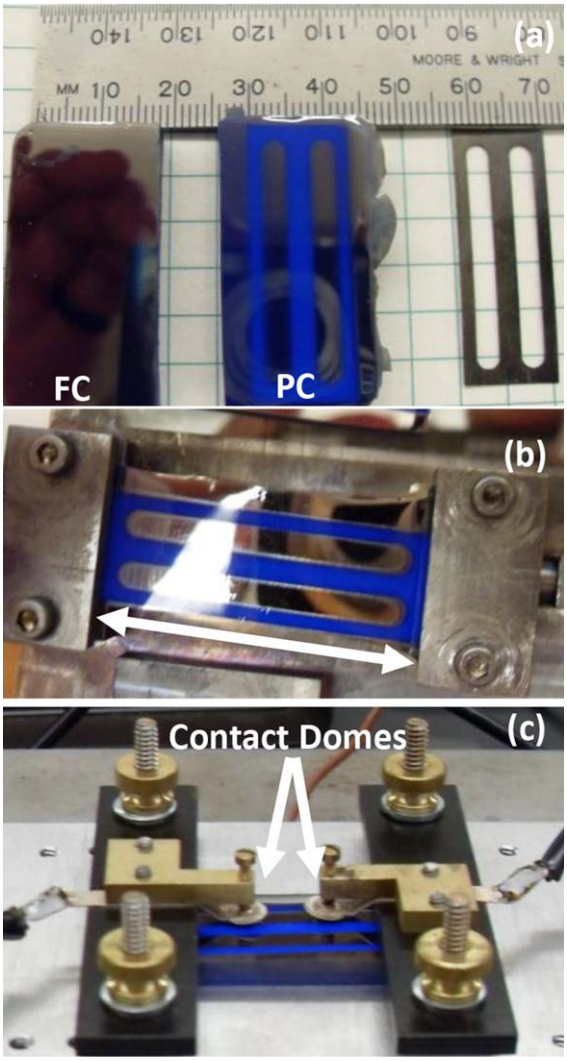

Figure 1. Masked deposition on samples with and without strain: (a) From left to right showing examples of FC and PC samples and the corresponding Al mask. (b) A pigmented RTV 655 sample loaded into the sample holder strained at 15%. Arrows indicate the direction of intended strain. No interfacial layer was introduced. (c) Custom-made sample holder with provisions for making electrical contact to the deposited Au films. [Color figure can be viewed in the online issue, which is available at wileyonlinelibrary.com.]

40 nm of carbon (C) was deposited at a rate of 0.5 A/s. Upon completion of the deposition the chamber was vented using pure argon (Ar) gas.

Thermal Evaporation. Polymer samples previously prepared were rinsed in IPA and dried immediately prior to a 10 s Ar plasma cleaning treatment in an Harrick plasma chamber. Samples were next loaded in a Denton Vacuum thermal evaporator and 40 nm of Au was evaporated onto relaxed (0% strain) RTV 655 samples as described previously.[8] The evaporator was given 20 min to cool down before venting with nitrogen (N_2) gas and carefully removing the samples. Thermal evaporation of C films was performed using an Ion Equipment Corporation evaporator with graphite rods as the carbon source. All prepared samples

(glass slides and polymers) were inspected by means of optical and electron microscopy techniques to confirm the continuity of the deposited thin films.

Electroless Deposition. Samples prepared in the section "Preparation of RTV 655 Substrates" were treated with an oxygen plasma step for 5 min prior to the electroless deposition process, rendering the surfaces hydrophilic. Deposition was performed both at room temperature and at $T = 4°C$ (to slow down the deposition rate) following protocols described in literature.[21] Initially, silver was deposited onto the membranes from a 0.029M $AgNO_3$ ammoniacal solution by a redox reaction. The membranes were rinsed with methanol followed by immersion in a basic Au-plating bath that contained $7.9 \times 10^{-3}M$ of a commercial plating solution $Na_3Au(SO_3)_2$ (Oromerse SO Part B, Technic, Inc., Providence, RI), 0.127M Na_2SO_3, and 0.625M formaldehyde at ~2°C. Samples were coated for 12 h followed by a 25% nitric acid soak for several minutes to remove residual elements.

BILAYER SYSTEM CHARACTERIZATION

Assessment of Au-RTV 655 Adhesion Strength

Water Tightness Test. The adhesion strength of the Au-RTV 655 bilayer was tested by placing Au sputter-coated samples in glass beakers while completely submerged in deionized water. The samples were kept submerged for 24 h at room temperature after which a probe sonicator (Fisher–Sonic Dismembrator-Model 300) was inserted in the glass beakers for 15 min operating at 40% of full power. The samples were then removed from the beakers and carefully inspected under a light microscope for any signs of peeling and delamination.

Temperature Cycling Test. Sputter-deposited Au-RTV 655 samples were positioned inside the heating chamber of a Mettler Toledo FP90 central processor heating unit and the unit's temperature was programmed to increase from ambient temperature to 100°C at a rate of 10°C/ min. The heating stage containing the sample was next positioned on the stage of a reflective light microscope and changes in the surface morphology were carefully monitored. A total number of 20 heat-cool cycles were performed. The heating/ cooling rate was kept constant for each cycle.

Optical Response of Bilayer System

The effect of substrate temperature and temperature-induced strain on the bilayer system was investigated by monitoring the reflection properties of the bilayer as a function of substrate temperature. For this, a 35 mW, 633 nm Oriel He–Ne laser was mounted on a tripod and positioned such that the angle of incidence was 54.72°. The reflectance spectra as a function of time was captured on a screen and photographed at regular intervals. The temperature was cycled between room temperature and 100°C at a rate of 10°C/min using a Thermolyne Type 1900 programmable hot plate. The heating cooling cycle was repeated ten times for each type of sample.

Electrical Response of Bilayer System

Current (I) vs. Voltage (V) Measurements. The room temperature I–V behavior of strained and relaxed Au + RTV 655 and Au + cover slip systems were investigated next. Current through the sputtered Au film was measured using a Keithley 196 System digital multimeter (DMM) while a set voltage was applied across the sample using a Hewlett Packard 6217A power supply and measured using a Fluke D 800 multimeter. The sample was held in place with a custom-built spring-loaded sample holder with provisions for making electrical contact to the conducting film (Figure 1(c)). The current was recorded as the voltage was increased from 1 V to a maximum of 40 V for all samples included (1) Au + cover slip (control), (2) Au + RTV 655 (0% strain), and (3) Au + RTV 655 (15% strain).

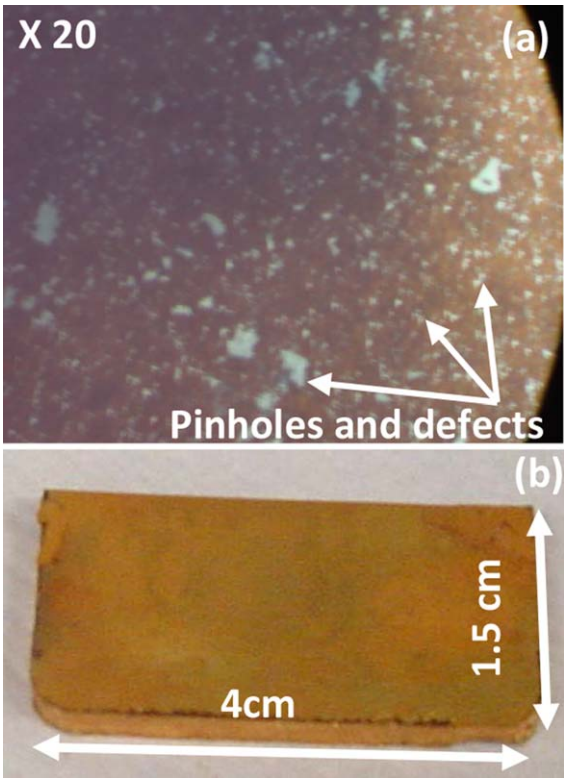

Figure 2. Electroless deposition onto RTV 655: Optical micrographs of electroless deposition of Au onto RTV 655 at (a) room temperature and (b) at 0°C for 12 h. Arrows indicate pinholes formed in the layer due to reaction rate too being too fast. Also, the deposited film did not pass 3M adhesion tape test. [Color figure can be viewed in the online issue, which is available at wileyonlinelibrary.com.]

Resistance (R) vs. Temperature (T) Measurements. The effect of substrate temperature on the resistance of the sputtered Au films mentioned in the section "Current (I) vs. Voltage (V) Measurements" was evaluated using a Keithley 196 System DMM connected to the custom-made sample holder shown in Figure 2. The resistance of the films was recorded be means of an ohmmeter at room temperature prior to heating. Using a Thermolyne Type 1900 hot plate the samples were heated to 120°C and allowed to cool to room temperature under ambient conditions. The resistance of the conducting layer was recorded as a function of temperature during the cooling cycle. The temperature of the Al stage that the sample was in direct contact with was monitored using a Fluke 52II thermocouple and was in close agreement with the temperature of the hot plate stage.

Table I. Summary of Sample Formations

Sample type	Deposition technique	Fixed strain during deposition (%)	Surface morphology	Optical behavior
Au (40 nm) + glass	Sputter/Thermal evaporation	NA	No buckles	Specular reflection
C (40 nm) + RTV 655 (3 mm)	Thermal evaporation	0	No buckles	Specular reflection
C (40 nm) + RTV 655 (3 mm)	sputtering	0	Multiaxial buckle	Concentric circles
Au (40 nm) + RTV 655 (3 mm)	Thermal evaporation	0	No buckles	Specular reflection
Au (40 nm) + RTV 655 (3 mm)	Sputtering	0	Multiaxial buckle	Concentric circles
		15	No buckles	Specular reflection
Au (40 nm) + RTV 655 (6 mm)	Sputtering	0	No buckles	Specular reflection
		15	No buckles	Specular reflection

Compression Behavior of Strained/relaxed RTV 655

Polymer substrates of thicknesses 3 mm and 6 mm were placed in a custom-made extender, such that the polymer was initially in the relaxed state. The substrate + extender system was then positioned on the stage of a Mark 10 tensile tester with a 200 lb force gauge, immediately under the compression rod. Care was taken to ensure that samples were taught but no strain was applied. The plate was set in direct contact with the polymer surface and the force gauge set to "zero". The force (compression) versus indentation (displacement into the polymer) was measured at a rate of 25 mm/min for each sample. The maximum permitted travel range (d_{Travel}) was set to 3 mm and 6 mm, respectively, for the two sample types. The measurements were then repeated for 3 mm and 6 mm thick substrates this time under a fixed uniaxial strain of 15%. All measurements were performed at room temperature. Table I summarizes the bilayer systems tested and the outcome of their characterization behaviors. Due to the unsatisfactory coating behavior, optical and electrical characterization was not performed on electroless coated samples.

RESULTS AND DISCUSSION

Electroless Deposition

The electroless deposition of RTV 655 substrates did not yield reproducible and uniform Au coatings. For this method, the thickness of the coating generally depends on the plating time. While a thick layer of Au (confirmed using spectroscopy) was indeed deposited, the adhesion was poor and the deposited layer contained large amounts of defects and pinholes suggesting a non-uniform reaction across the surface of the polymer leading to imperfections in the deposition as shown in Figure 2(a). Additionally, the fast reaction rate associated with this technique made it difficult to have precise control over the deposited thickness and non-uniform coating thickness was observed as shown in Figure 2(b). The deposition was repeated while the solutions containing the samples were kept in a refrigerated environment and the reaction/deposition rate for the solution concentration used here was still too fast. While this method is suitable for rapid large area coatings, it is unsuitable in its current state for coating nm-thick films on elastomeric substrates. In some cases both sides of the polymer sample was coated which was an undesired outcome. Although defects were present in the deposited film, the continuous regions of the film were smooth and the adhesion strength was the weakest when compared to the sputtering and thermal evaporation techniques. Coated regions delaminated easily upon contact with other surfaces. Given that the adhesion between the Au layer and the RTV 655 substrate was very weak, optimization of the solution concentrations and plating times to achieve desired Au thicknesses was not pursued.

Sputtering versus Thermal Evaporation of Thin Films

Substrate relaxed (0% strain): Despite significant thermal expansion coefficient (TEC) mismatch between RTV 655 and Au ($\rho_{\text{RTV 655}} = 330 \times 10^{-6}$ μm/m K,[22] $\rho_{\text{Au}} = 14.2 \times 10^{-6}$ K^{-1})[23] thermal evaporation of Au thin films onto 3-mm thick RTV 655 elastomeric substrates did not give rise to buckle formation which contradicts previous reports.[15,17] The as-deposited films were smooth and homogeneous as confirmed by atomic force microscopy,[8] scanning electron microscopy, and optical reflection analysis of the bilayer systems. This, however, was not the case for Au films sputter-deposited onto 3 mm thick RTV 655 substrates (shown in Figure 3) where herringbone multiaxial buckles formed. This is typically a sign of isotropic biaxial compressive stress in the as-

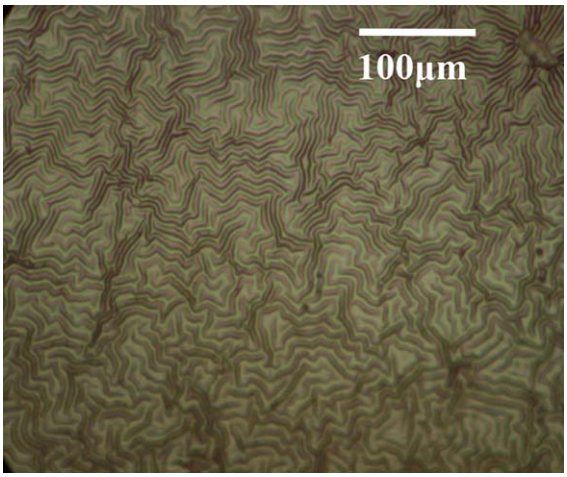

Figure 3. Herringbone buckles in an Au+RTV 655 bilayer system: Optical microscope image of 40 nm sputter-deposited Au onto a relaxed (0% strain) RTV 655 substrate of 3 mm thickness. Herringbone buckles representing isotropic stress were formed. No interfacial layer was deposited. [Color figure can be viewed in the online issue, which is available at wileyonlinelibrary.com.]

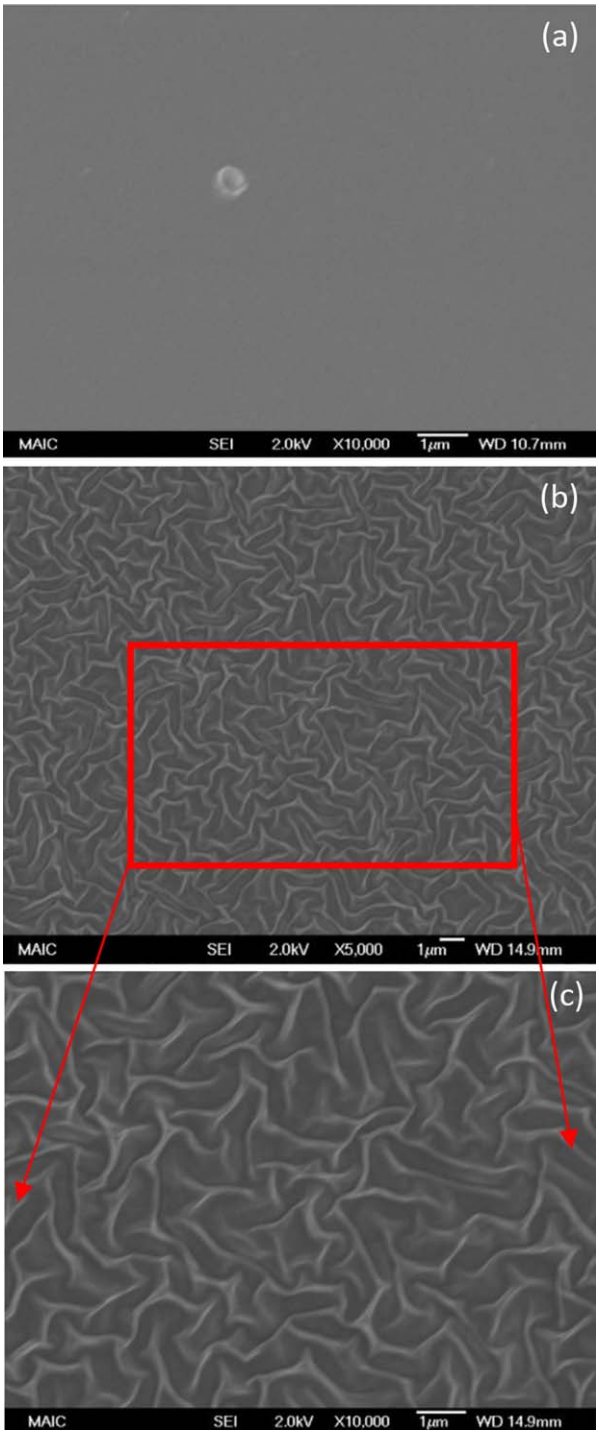

Figure 4. Herringbone buckles in a C + RTV 655 bilayer system: (a) SEM image of thermally evaporated C onto relaxed RTV 655 substrate. No buckles were formed in spite of the thermal expansion coefficient mismatch and the high temperature nature of the thermal evaporation process. (b) SEM image of 40 nm ion beam-deposited C onto relaxed (0% strain) RTV 655 substrate showing formation and appearance of herringbone buckles. (c) Magnified image of (b) showing the biaxial nature of the buckles. [Color figure can be viewed in the online issue, which is available at wileyonlinelibrary.com.]

deposited thin film and compressive stress in such films is known to induce spontaneous wrinkling.[17] The buckling periodicity is clearly on the micron scale. Thermally evaporated carbon films on 3-mm thick RTV 655 substrates did not produce buckles [see Figure 4(a)] even though a significant TEC mismatch between these two materials ($\rho_C = 1.5–7 \times 10^{-6}$ K^{-1},[24] $\rho_{\text{RTV 655}} = 330 \times 10^{-6}$ K^{-1})[20] exists.

These results suggest that TEC mismatch alone cannot support the appearance of buckles as stated previously.[15,17] The brief plasma cleaning treatment prior to thermal evaporation is not expected to modify the surface mechanical properties and is unlikely to have contributed to these results. Biaxial compressive stress was also observed in the case of ion beam-deposited C films on 3-mm thick RTV 655 substrates as seen in Figure 4(b) and (c). Since both ion beam and sputtering deposition techniques create species with high landing energy buckle formation and presence of compressive stress is not a surprise outcome.[20] On the other hand, thermal evaporation typically results in ionic species with low landing energies thus creating a smooth and flat surface. It is hypothesized that the high landing energy of the sputtered ions as well as the compressibility of a thin elastomeric substrate has lead to formation of buckles. Microscope slides and cover slips coated simultaneously were thoroughly inspected by means of optical microscopy and reflection analysis and did not reflect the same pattern formation seen in the film + RTV 655 system further suggesting that the mechanical properties and compliance of the substrates are key parameters that heavily influence the coating morphology. The difference in buckle periodicity between Figures 3 and 4(b) are attributed to the differences in the landing energies as well as the Young's moduli of the coatings.

Substrate under uniaxial strain (15% strain): film buckling did not occur on sputter-deposited RTV 655 substrates pre-stretched to a strain of 15% when examined by optical microscope and by surface reflection studies. In these cases the as-deposited film (prior to release of fixed strain) was continuous and smooth with a specular reflection across the sample. Upon release and ultimate removal of the strain however periodic and uniform "accordion" style buckles appeared in a direction perpendicular to the elongation axis and are shown in Figure 5 for different samples. Cracks parallel to the direction of the elongation are attributed to stress relief also known as the Poisson effect[16] as indicated by arrows in Figure 5(b)–(d). A fixed uniaxial strain of 15% has led to the formation of highly ordered nanometer-scale buckles. Figure 5(b) shows a magnified image of buckles shown in Figure 5(a) while Figure 5(d) shows a magnified image of Figure 5(c). While both samples [Figure 5(a) and 5(c)] were created with a 15% fixed strain, a slight difference in the periodicity of the two films can be seen. Due to the nature of the polymeric sample loading and inevitable variations in grip mechanics some inconsistencies between different samples is expected. The regions were the Au film has torn due to the Poisson's effect show exposed polymer substrate and beam charging during imaging has occurred.

Effect of Strain on Mechanical Response of Elastomer

Compression tests performed on the 3 mm thick and 6 mm thick RTV 655 substrates help explain the influence of substrate

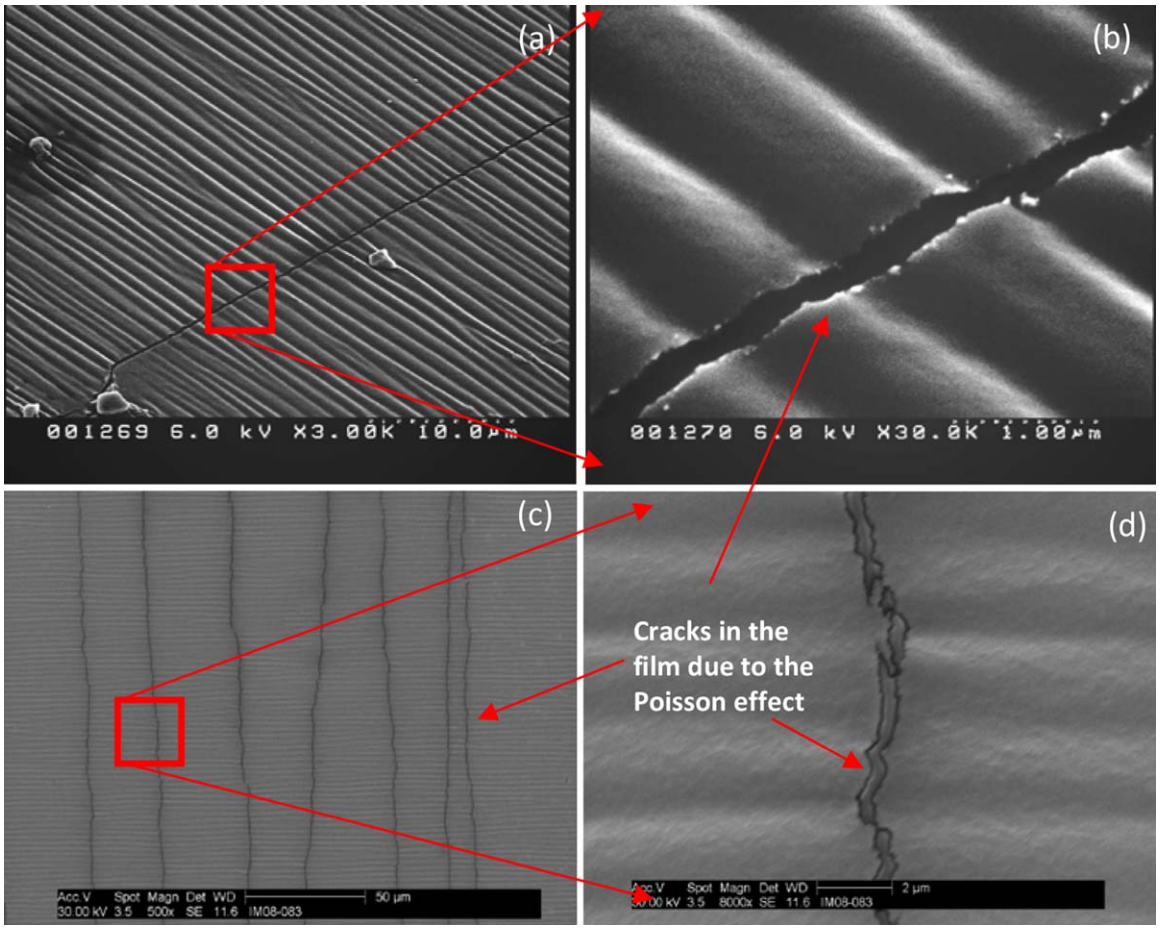

Figure 5. Uniaxial buckle formation in Au + RTV 655 system under fixed strain: SEM images of (a) 40 nm of Au sputter-deposited onto 15% strained RTV 655. Upon release of the strain a highly ordered periodic accordion-style buckle array appears. Arrows in (b) and (d) indicate cracks formed as a result of the Poisson effect that could contribute to the electrical resistance behavior. [Color figure can be viewed in the online issue, which is available at wileyonlinelibrary.com.]

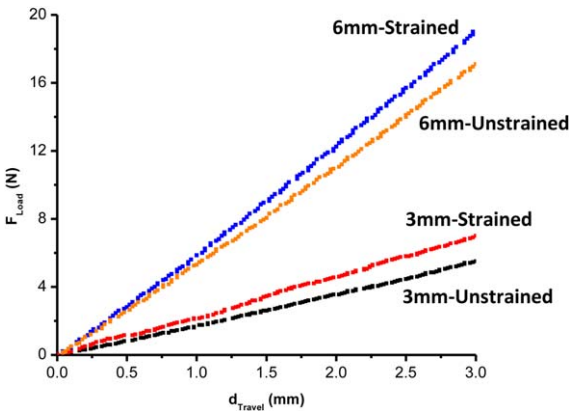

Figure 6. Effect of strain on polymer stiffness: figure shows typical compression behavior for a strained and unstrained RTV 655 substrate of 3 mm and 6 mm thickness under atmospheric conditions. The strained substrates appear stiffer compared to the unstrained substrates while thicker substrates also show an increase in "apparent" stiffness. [Color figure can be viewed in the online issue, which is available at wileyonlinelibrary.com.]

thickness and stiffness on the compression properties of the elastomer that were mentioned in the section "Sputtering versus Thermal Evaporation of Thin Films". The force–displacement (*F–d*) behavior of 15% strained and relaxed (0%) 6 mm and 3 mm thick substrates are compared in Figure 6. In both cases, the strained sample is significantly stiffer and shows less compliance compared to the unstrained sample. An increase of a factor of two in the substrate thickness results in a material rigidity increase of at least a factor of three strongly suggesting that the "apparent" stiffness of the elastomeric substrate at the time of metallization directly impacts the profile and pattern of the as-deposited thin film. This explains why depositions on "hard" substrates, e.g., glass slides and strained polymer samples lead to smooth buckle-free film coverage while deposition on relaxed "soft" substrates lead to buckle formations.

The theoretical description of buckling of metal films on elastomeric substrates suggests that the buckle wavelength (periodicity) depends on the Young's moduli of the metal film and the elastomer as well as the film thickness.[25] This explains the observed differences in buckling periodicity and morphology between the Au-coated and C-coated RTV 655 substrates.

Effect of Temperature on Reflection Pattern

(a) Herringbone (amorphous) buckles: the reflection pattern formed by illuminating the sample in Figure 3 (relaxed

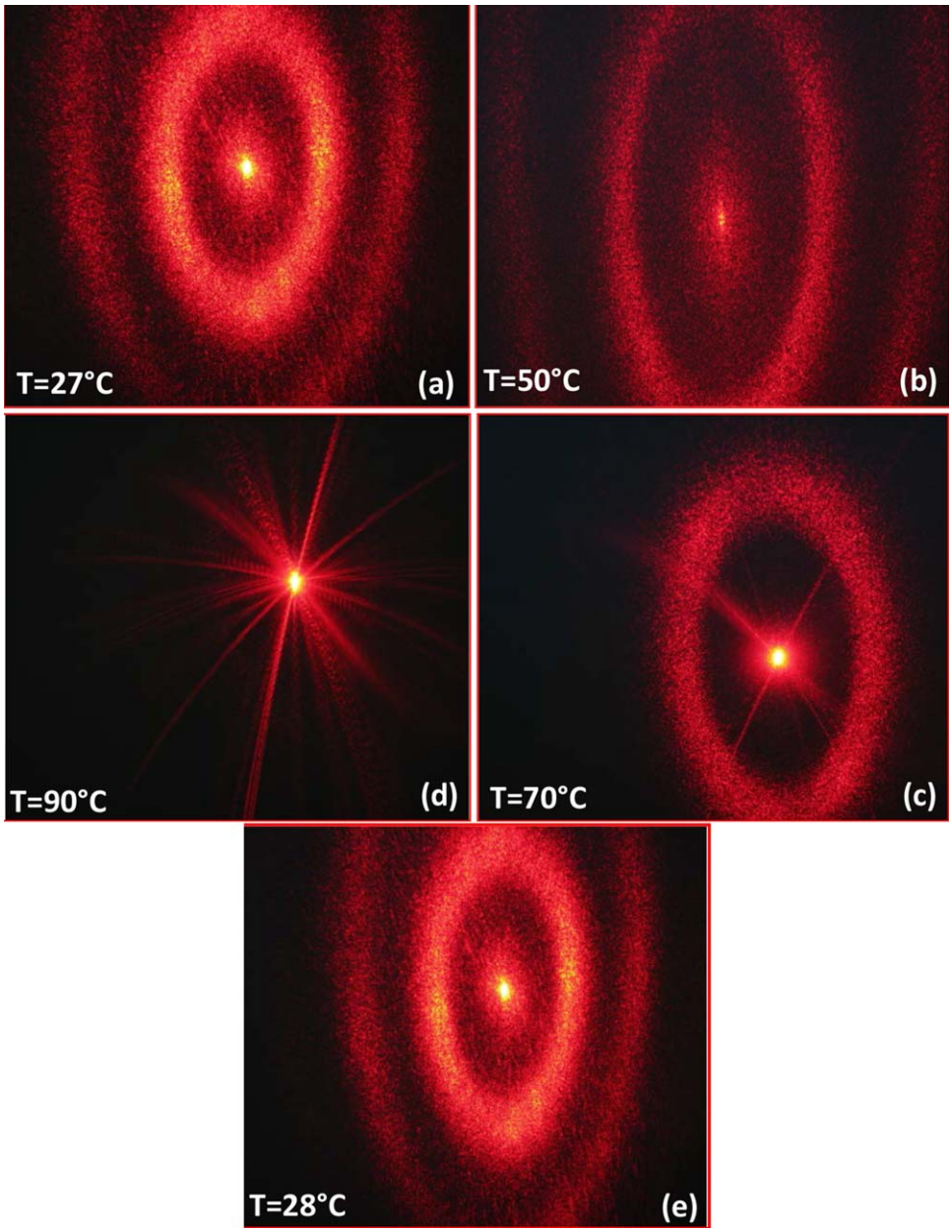

Figure 7. Effect of thermal cycling on optical behavior-isotropic buckles: diffraction pattern from herringbone buckles (shown in Figure 4) as the Au–RTV 655 system is heated gradually from (a) room temperature to 100°C, specular reflection occurs at (c) approximately 90°C. Further cooling of the bilayer system towards ambient conditions shows reappearance of higher order interference bands shown in (d) and (e). [Color figure can be viewed in the online issue, which is available at wileyonlinelibrary.com.]

Au + RTV 655) sample at room temperature consists of a series of concentric rings demonstrating the reflection pattern resulting from biaxial stress in the film and is shown in Figure 7. As the substrate temperature is increased from 27°C [Figure 7(a)] to a maximum temperature of 100°C the Au + RTV 655 bilayer system expands and expansion in the *X*–*Y* plane causes a gradual disappearance of the higher order rings. This continues until finally at $T = 90$°C the Au film is completely planarized and a specular reflection is observed [Figure 7(d)]. Upon cooling of the system the higher order rings gradually reappear with the same characteristics as the heat cycle. At room temperature [Figure 7(e)], the interference rings (hence the buckles) fully reappear with the same periodicity as before. The heat/cool cycle was repeated 10 times for each sample and the planarization temperature as well as the rate of disappearance/reappearance of the higher order rings was consistent with previous observations each time suggesting a strong adhesion between sputter-deposited Au film and the surface of the RTV 655 in the absence of an interfacial layer.

(b) Accordion buckles: the 15% uniaxially strained Au + RTV 655 bilayer samples were subject to the same heat/cool cycle test described previously in (a) and the results are shown in Figure 8. At room temperature ($T = 23$°C) the reflection pattern consists of a series of bright spots shown in Figure 8(a). As the substrate

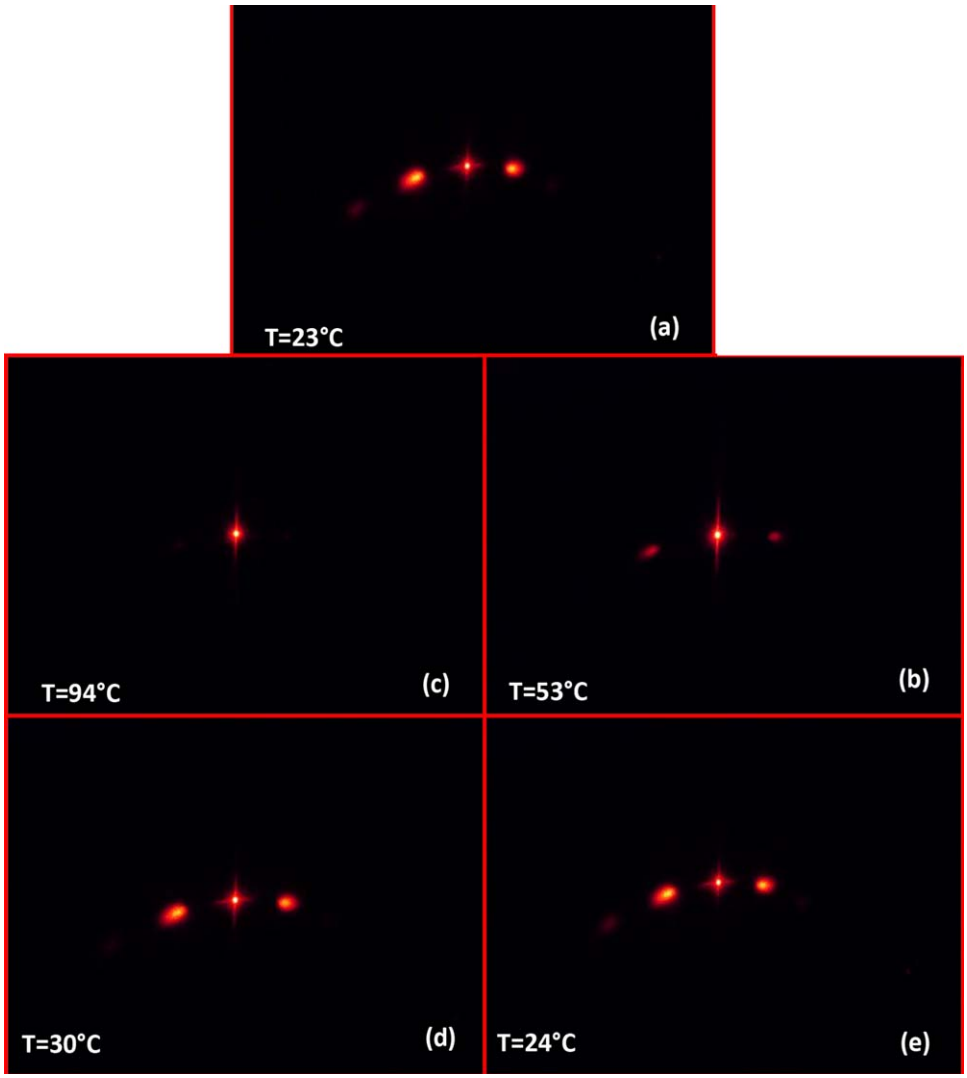

Figure 8. Effect of thermal cycling on optical behavior-uniaxial buckles: diffraction pattern from 40 nm Au on 15% strained RTV 655 substrates. As the bilayer is thermally cycled from (a) 23°C (room temperature) to 100°C the diffraction pattern shows specular reflection at (c) 94°C and continues to recover the higher order interference as cooled back to (e) room temperature. [Color figure can be viewed in the online issue, which is available at wileyonlinelibrary.com.]

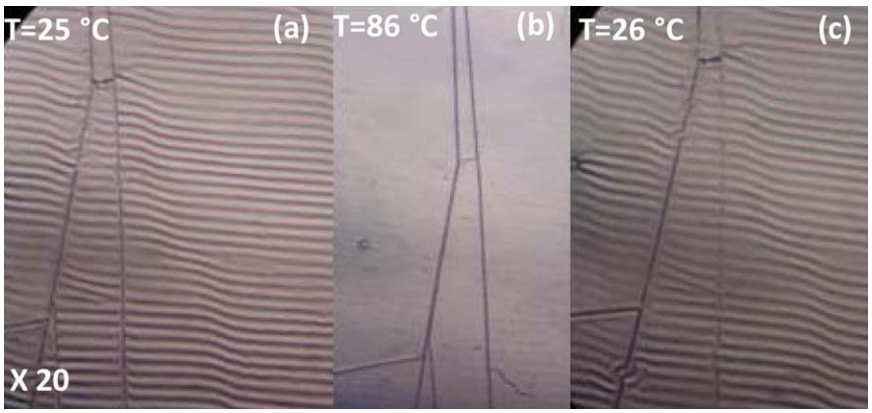

Figure 9. Water tightness test: optical images of Au + RTV 655 bilayer sample thermally cycled after exposure to an aqueous bath. (a) Buckles present at room temperature reappear after heating/cooling cycle shown in (b), and (c) suggesting strong adhesion between the two layers. [Color figure can be viewed in the online issue, which is available at wileyonlinelibrary.com.]

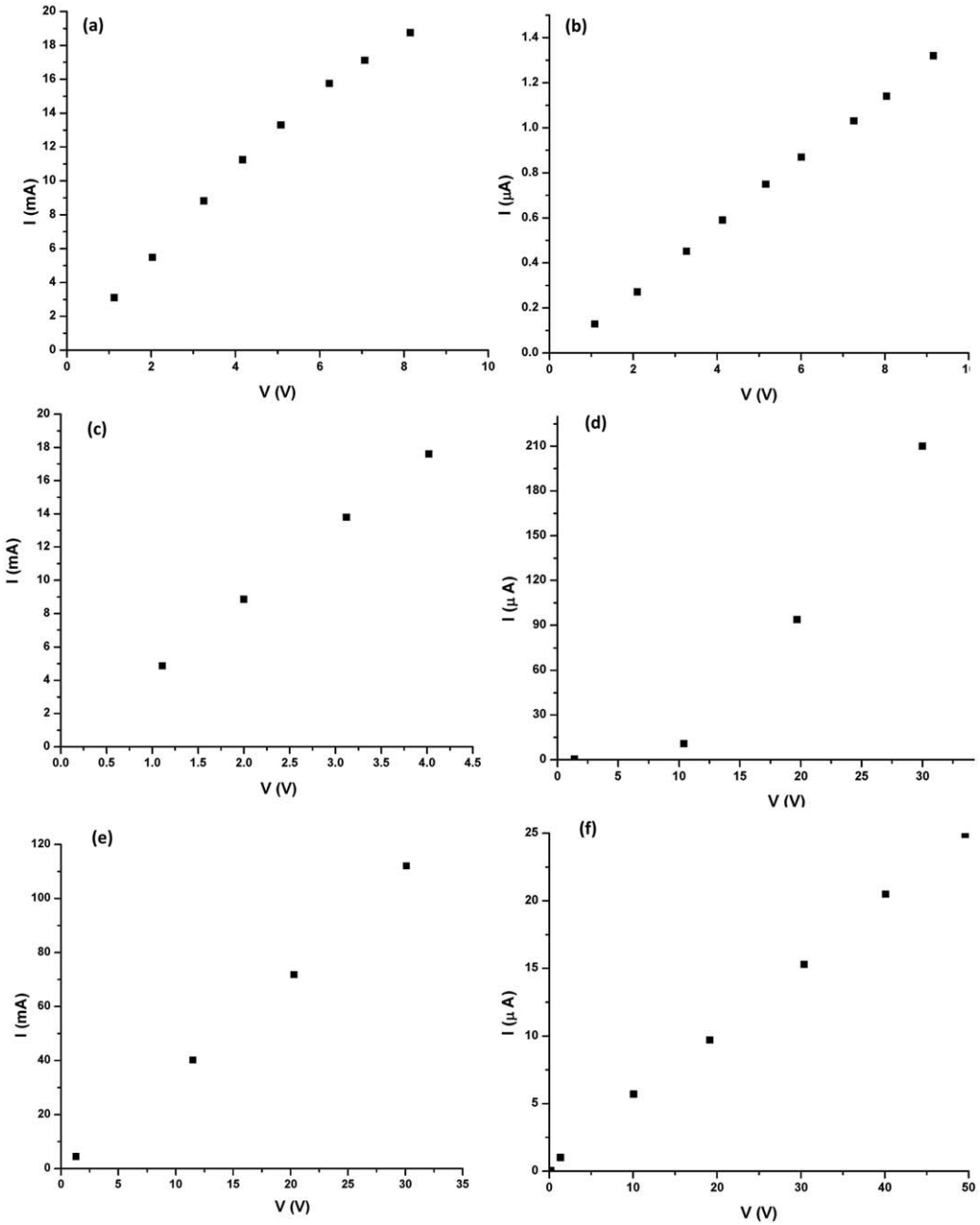

Figure 10. Room temperature *I–V* behavior of bilayer systems: *I–V* profile of (a) 40 nm Au + RTV 655 FC substrate with 0% strain, (b) 40 nm Au + RTV 655 PC with 0% strain, (c) 40 nm Au + RTV 655 FC substrate with 15% strain, (d) 40 nm Au + RTV 655 PC with 15% strain, (e) 40 nm Au + glass FC and (f) 40 nm Au + glass PC. The room temperature profiles of all bilayer systems show a linear and Ohmic behavior with resistance variations reflecting individual geometrical differences.

temperature increases from ambient (23°C) to 100°C, the uniaxial buckles begin to disappear gradually [Figure 8(b)] until at ~94°C the film is fully planarized. As the system is cooled, once again, the buckles reappear with the same periodicity as before and the cycling tests lead to consistent results each time.

In both cases (a) and (b) mentioned above, the sputter-deposited Au films appear to be strongly bound to the polymeric substrate despite the lack of an adhesion-promoting interfacial layer. Published reports that plasma treatment of polysiloxane leads to better adhesion[26] supports this finding. It has also been reported that the energetic sputtered ionic species can and do penetrate the top few nanometers of soft substrates such as elastomers[27] and "intermixing" between film and substrate occur. It is believed that this mechanism of ionic sub-plantation during film growth can lead to buckling[28] and that thermal stress upon cooling is not the only mechanism for buckle formation. Water tightness tests performed before and after thermal cycling confirmed that the sputter-coated Au film is strongly attached to the top layer of the elastomer and the two layers respond to the thermally induced stress/ strain

together as one unit. While the exact mechanism of interaction and intermixing between the two layers is not fully understood, it is clearly related to the energetic ions (C and Au) bombarding the RTV 655 surface and not thermal stress since buckles were not observed during thermal evaporation. Furthermore, sputter deposition on 15% strained RTV 655 samples resulted in smooth buckle-free films. Uniaxial buckles were only formed upon release of the strain. The compression tests shown in Figure 6 demonstrate that a 15% strained film has a greater "apparent" stiffness compared to the unstrained polymer of the same thickness as judged by the slope of the graph. A typical heat/cool cycle pre/post water tightness test is shown in Figure 9 where upon cooling, the buckles reappear with the same periodicity and at the same locations as before. This further supports the notion that upon sputtering, ionic species of Au (and C) are "embedded" into the top nm-thick layer of the elastomer and the deposited film.

I–V and *R–T* Behavior of Buckled Films

Typical *I–V* profiles for 0% and 15% strained Au + RTV 655 bilayer systems are shown in Figure 10 where Figure 10(a) and (b) shows representatives of *I–V* responses measured for 0% strain (FC and PC) of 40 nm Au + RTV 655 bilayer systems. The typical *I–V* profile for 15% strained 40 nm Au + RTV 655 FC and PC are shown in 10(c) and (d), respectively, while *I–V* behavior of Au + glass (control) for both FC and PC are shown in 10(e) and 10(f), respectively. All *I–V* profiles of the different bilayer systems demonstrate Ohmic (linear) behavior and differences in the measured resistance magnitudes are attributed to the differences in morphology and surface area of the individual coated samples. The response of the measured film resistance to increasing substrate temperature for 0% and 15% strained PC samples showed interesting and distinct behaviors that could be utilized for sensor development. The increase of substrate temperature for 0% strained PC samples [Figure 11(a)] resulted in a gradual and nonlinear temperature response. Four separate samples were measured and (slight) differences in geometry and metal–polymer boundary conditions resulted in differences among the samples that were tested. Lower points of Figure 11(a) are magnified in Figure 11(b) and individual *R–T* profiles for each sample can be seen. Overall, the gradual nonlinear increase in resistance is consistent for all samples. The increase in resistance for these systems is attributed to (a) increased strain in the bilayer and (b) the increase in resistivity of the Au film. In this work, the polymer substrate is assumed to be a homogeneous material and thus in response to the increased temperature the bilayer system expands gradually and uniformly giving rise to a continuous increase in resistance. Due to the complexity of the system, the contributions from each mechanism cannot be quantified in its current form. In the case of 15% strained samples with narrow parallel channels [Figure 11(c)] however, at temperatures close to the planarization temperature (noted during reflection studies discussed in the section "Effect of Temperature on Reflection Pattern") pronounced step change in the *R–T* behavior can be seen. The overall *R–T* behavior observed was consistent for each measurement run. The *R–T* profiles of two separate samples are presented here. It is hypothesized that in the case of the 15% strained samples the planarization of the buckles contributes to the increased resistance and at a critical

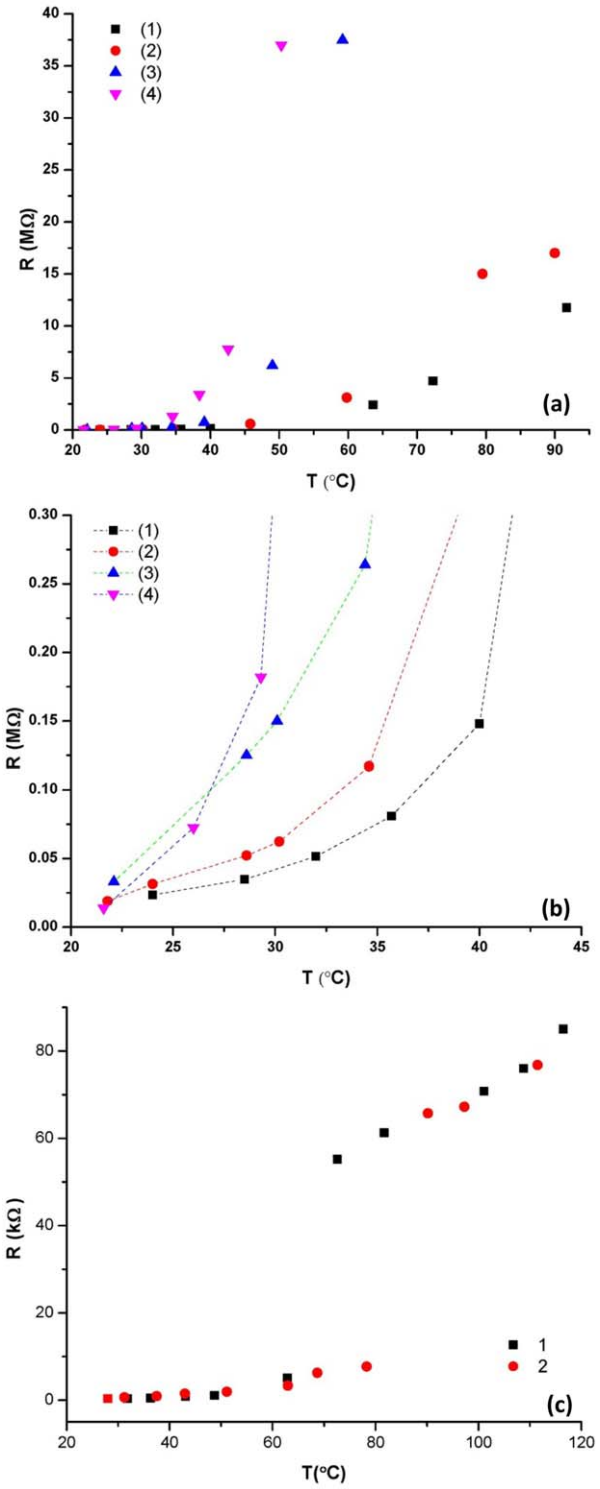

Figure 11. *R–T* behavior of 40 nm Au + RTV 655 PC bilayer systems: *R–T* behavior of (a) 0% strained bilayer systems demonstrating a strong non-linearity where the lower points have been highlighted in (b). Measurement was repeated for four separate samples indicated by "1", "2", "3", and "4" on the graph. The non-linearity of 15% strained system shown in (c) where a sharp step change in the resistance has been detected. Measurement was repeated for two separate samples indicated by "1" and "2" on the graph. [Color figure can be viewed in the online issue, which is available at wileyonlinelibrary.com.]

temperature a sharp step-like transition in R is observed. This feature is particularly pronounced for Au + RTV 655 bilayer systems that contained narrow parallel channels shown here [Figure 1(b)]. While increased resistivity and thermal expansion are still plausible arguments for the increase in resistance, the sharp step change in the R–T behavior suggests a new mechanism is contributing to the electrical response. The 0% strained samples typically show resistances much greater than those seen for the strained substrates. The higher resistance values for the 0% strained systems reflects changes in the sputtered Au film, perhaps even formation of cracks as a result of the expansion. The lower resistance and step-height change seen for the strained bilayer systems at the temperature of planarization suggests that the unfolding of the buckles may be dominating the R–T response. The R–T response is expected to be strongly dependent on the buckle wavelength and therefore can be adjusted to appear at a preset temperature. This phenomenon can be taken advantage of in the design of a thermally activated stress/strain sensor.

SUMMARY AND CONCLUSION

Sputter-deposited thin films on elastomeric substrates demonstrate strong adhesion without delamination despite the lack of an interfacial adhesion layer. Buckle formation in deposited thin films seems to be dominated by landing energy and "apparent" substrate stiffness rather than thermal expansion coefficient mismatch between deposited thin film and elastomeric substrate. In both cases thermally evaporated C and Au films lead to smooth surfaces while sputtered films resulted in buckled morphology and appearance. Thermally induced changes to the buckled Au layer lead to distinct optical and electrical behavior that is potentially tunable and can be designed to fit a desired application window thus forming the foundation for sensor applications.

ACKNOWLEDGMENTS

The first author is the recipient of the 2008 APS Hildred Blewett Award and would like to acknowledge the agency for financial support. The funders had no role in study design, data collection and analysis, decision to publish, or preparation of the manuscript. The corresponding author would like to acknowledge John Daffron, Dept. of Physics, University of Memphis for instrumentation support. Also, thanks to Kerry Sieben, MAIC, UF and Lou Boykins, IMC, UoM for microscopy assistance.

REFERENCES

1. Huang, H.; Spaepen, F. *Acta Mater.* **2000**, *48*, 3261.
2. Gubanski, S. M.; Vlastos, A. E. *Power Deliv.* **1990**, *5*, 1527.
3. Reynders, J. P.; Jandrell, I. R.; Reynders, S. M. *IEEE Trans. Dielectr. Electr. Insul.* **1999**, *6*, 620.
4. Wong, E. W.; White R. C. *Biomater. Med. Devices Artif. Organs.* **1979**, *7*, 283.
5. Boland, J. J. *Nat. Mater.* **2010**, *9*, 790.
6. Misiakos, K.; Petrou, P. S.; Kakabakos, S. E.; Vlahopoulou, M. E.; Tserepi, A.; Gogolides, E.; Ruf, H. H. *Microelectr. Eng.* **2006**, *83*, 1605.
7. Sabri, F.; Marchetta, J. G.; Sinden-Redding, M.; Habenicht, J. J; Chung, T. P.; Melton, C. N.; Hatch, C. J.; Lirette, R. L. *PLoS ONE* **2012**, DOI: 10.1371/journal.pone.0045719.
8. Sabri, F.; Werhner, T.; Hoskins, J.; Schuerger, A. C.; Hobbs, A. M.; Barreto, J.A.; Britt, D.; Duran, R.A. Thin film surface treatments for lowering dust adhesion on Mars Rover calibration targets *Adv. Space Res.* **2008**, *41*, 118.
9. Xiang, Y.; Li, T.; Suo, Z.; Vlassak, J. J. *Appl. Phys. Lett.* **2005**, *87*, 161,910.
10. Garbassi, F.; Morra, M.; Occhiello, E. In Polymer Surfaces: From Physics to Technology, Wiley: Chichester, **1998**, pp 235–288.
11. Strobel, M.; Lyons, C. S.; Mital, K. L. In Plasma Surface Modification of Polymers: Relevance to Adhesion, VSP Press: Zeist, Netherlands, **1994**.
12. Jones, J.; Lacour, S. P.; Wagner, S.; Suo, Z. *J. Vac. Sci. Technol. A* **2004**, *22*, 1723.
13. Chambers, C.; Lacour, S. P.; Wagner, S.; Suo, Z.; Huang, Z. *MRS Proc.* **2003**, *769*, 325.
14. Li, W. T.; Charters, R. B.; Luther-Davies, B.; Mar, L. *Appl. Surf. Sci.* **2004**, *233*, 227.
15. Chen, X.; Hutchinson, J. W. *Script. Mater.* **2004**, *50*, 797.
16. Chen, X.; Hutchinson, J. W. *J. Appl. Mech.* **2004**, *71*, 597.
17. Bowden, N.; Brittain. S.; Evans, A. G; Hutchinson, J. W.; Whitesides, G. M. *Nature* **1998**, *393*, 146.
18. Paunovic, M.; Schlesinger, M. Fundamentals of Electrochemical Deposition, John Wiley & Sons: Hoboken, **2006**.
19. Smith D. Thin-Film Deposition: Principles and Practice, McGraw-Hill, **1995**.
20. Freund L. B.; Suresh, S. Thin Film Materials: Stress, Defect Formation and Surface Evolution, Cambridge University Press, **2004**.
21. Wirtz, M.; Miller, S. A.; Martin, C. R. *Int. J. Nanosci.* **2002**, *11*, 255.
22. Rogers, J. A.; Jackman, R. J.; Schueller, O. J. A.; Whitesides, G. M. *Appl. Optics* **1996**, *35*, 6641.
23. Thornton, J. A.; Hoffman, D. W. *Thin Solid films* **1989**, *171*, 5.
24. Silva, S. R. P. *Properties of Amorphous Carbon*, The Institution of Engineering and Technology London, **2003**, pp 159.
25. Khang, D.-Y.; Rogers, J. A.; Lee, H. H. *Adv. Funct. Mater.* **2009**, *19*, 1526.
26. Li, W. T.; Charters, R. B.; Luther-Davies, B.; Mar, L. *Appl. Surf. Sci.* **2004**, *233*, 227.
27. Manzoor, M. U.; Tuinea-Bobe, C. L.; McKavanagh, F.; Byrne, C. P.; Dixon, D.; Maguire, P. D.; Lemoine, P.; *J. Phys. D: Appl. Phys.* **2011**, *44*, 1.
28. Robertson, J. *Diamond Relat. Mater.* **1993**, *2*, 984.